Lemström, Ida; Polojärvi, Arttu; Tuhkuri, Jukka

Model-scale tests on ice-structure interaction in shallow water, Part I

Published in:
Marine Structures

DOI:
10.1016/j.marstruc.2021.103106

Published: 01/01/2022

Document Version
Publisher's PDF, also known as Version of record

Marine Structures 81 (2022) 103106

Contents lists available at ScienceDirect

Marine Structures

journal homepage: www.elsevier.com/locate/marstruc

Model-scale tests on ice-structure interaction in shallow water, Part I: Global ice loads and the ice loading process

Ida Lemström *, Arttu Polojärvi, Jukka Tuhkuri

Aalto University, School of Engineering, Department of Mechanical Engineering, P.O. Box 14300, FI 00076, Aalto, Finland

ARTICLE INFO

Keywords:
Ice mechanics
Arctic technology
Ice-structure interaction
Ice load
Model-scale experiments
Offshore structures

ABSTRACT

Laboratory-scale experiments on ice-structure interaction process in shallow water were performed by pushing a ten-meter-wide ice sheet against an inclined structure of the same width. Seven experiments were performed in three series: In one of the series, the compressive and flexural strengths were both about 50 kPa, in the two other test series the ice strength was two and four times higher. The ice thickness was about 50 mm in all experiments. The loading process showed two phases: the ice load on the structure (1) first increased linearly with a rate that was constant for all experiments, after which (2) the loading process reached a steady-state phase with approximately constant load. The magnitude of ice loads was not proportional to ice strength, as the weakest ice yielded higher loads than the ice having twice its strength. The ice rubble grounded in all experiments, but the bottom carried only a small portion of the load. The load records could be normalized by a factor combining the weight and the characteristic length of the intact ice. Based on the normalization, a model explaining the loading process was derived; the weight of the incoming ice has a dominant role during phase (1), while buckling explains the change in the process to phase (2) when the ice is strong enough. The loading process for the weakest ice was different from that for the other two ice types used. For example, instead of forming a rubble pile consisting of distinct ice blocks, weakest ice formed a dense pile of slush. The normalized ice load data highlighted the differences in the loading process.

1. Introduction

Ice loads on offshore structures are due to an ice-structure interaction process. In the case of an inclined structure, the process starts by an intact ice sheet moving against the structure and failing into ice blocks, which form an ice rubble pile. Many offshore structures, such as ice barriers, artificial islands, and platforms, are wide and operate in shallow water. Under these conditions, the rubble pile grounds, that is, it comes into contact with the seabed. Grounding may affect the ice loading process and it has been suggested that grounded rubble piles protect the structure from high ice loads, since the loads are partially transmitted to the seabed [1–3]. Such observations are from conditions, where freezing could have occurred between the ice blocks of the rubble. In a case of a pristine and continuous ice loading process with no consolidation, however, grounding may increase in magnitude of ice loads [4].

Model-scale testing is the state-of-the-art method for predicting the performance of and the ice loads on structures in ice. When compared to full-scale experiments, model-scale experiments allow a control of variables, are less expensive, and easier to perform. There are, however, limitations to model-scale testing to and scaling of the results to full-scale. Model-scale testing involves conditions of similitude and the assumption that a model ice can reproduce the mechanical behavior of full-scale ice. Model-scale

* Corresponding author.
E-mail address: ida.lemstrom@aalto.fi (I. Lemström).

https://doi.org/10.1016/j.marstruc.2021.103106
Received 21 May 2021; Received in revised form 27 September 2021; Accepted 13 October 2021
Available online 28 October 2021

testing techniques and the scalability of the model-scale results are reviewed by Riska et al. [5] and von Bock und Polach and Ehlers [6], whereas the properties of model ice are discussed, for example, by Zufelt and Ettema [7], Li and Riska [8], and von Bock und Polach et al. [9,10].

Several field observations of grounded rubble piles, formed both against a shore or an offshore structure, have been made, as summarized by Barker and Timco [11]. However, observations on the rubbling processes in shallow water are rare [12,13]. Laboratory-scale experiments on shallow water ice-structure interaction have been conducted earlier by several authors. In their experiments on the rubble field formation around a sloping island, Yoshimura and Inoue [14] focused on the general characteristics of the ice loading process and on the ice loads. The experiments showed that the ice sheet failed irregularly and non-simultaneously against the gravel island and the rubble formation process around the gravel island in the model tests was found to have realistic failure characteristics. The flexural strength was varied only between $12 \cdots 14$ kPa, but the effect of it was not reported. Timco et al. [15], on the other hand, investigated the load transmission through the rubble pile on a vertical structure and a submerged berm. In their experiments, the flexural strength was varied between $10 \cdots 41$ kPa and no clear trend in the load apportioning of the strength was observed. The experiments indicated that very small horizontal forces are primarily transmitted to the berm, but as the applied force increases, the load became mainly applied on the structure. Karulin et al. [16] studied the effect of the water depth and ice thickness on the rubble pile-up in front of a caisson-type platform and on the ice loads acting on it. They observed increased structure loads during the initial stage of the interaction process in shallow water, when compared to experiments in deep water. The ice strength was not varied in their experiments. Evers and Weihrauch [17] and Repetto et al. [18,19] performed model-scale tests on different types of ice barriers in order to evaluate their performance and to establish design ice loads. Evers and Weihrauch [17] varied the thickness of the ice, but used a constant ice strength, while Repetto et al. [18,19] varied the flexural strength of the ice between $35 \cdots 110$ kPa. Repetto et al. [19] found a linear trend between block size and ice thickness, but no clear effect of the flexural strength on the ice block size and breaking length was observed. However, the flexural strength was varied simultaneously with the ice thickness and thus, it was not straightforward to examine the effect of flexural strength alone. Furthermore, Serré et al. [20,21] and Lu et al. [22] studied the load distribution, failure mechanisms and parameter effects on a downward sloping offshore structure. In their experiments, a variation of $46 \cdots 58$ kPa in the flexural strength did not lead to any difference in the loads and in the accumulation of ice rubble.

The width of the structure in all of the aforementioned experiments was smaller than 1.5 m. Timco [23], on the other hand, studied the effect of different parameters, such as structure width, ice thickness and the flexural strength of ice, on the loads on a wide upwards sloping structure based on model-scale experiments in deep water. In their experiments, the flexural strength of the ice was varied between $4 \cdots 68$ kPa, but an increase in the flexural strength showed only very sight increase in the ice loads. Bridges et al. [24] performed experiments on a structure of the width 5 m. In their experiments, the water depth was kept constant at 0.33 m, while the ice thickness varied between $0.04 \cdots 0.06$ m and the flexural and compressive strength between $43 \cdots 83$ kPa and $76 \cdots 148$ kPa, respectively. Unlike the other authors, Bridges et al. [24] observed that an increase in ice strength clearly increased the maximum pile height and ice encroachment length.

As mentioned above, previous model-scale experiments on shallow water ice-structure interaction have been conducted on structures with widths below 1.5 m. Although Bridges et al. [24] performed experiments with a wider structure, their focus was on ice encroachment and no ice loads were measured. In addition, the previous laboratory-scale work on shallow water ice-structure interaction, even when the ice strength have been varied, have been conducted with ice having the flexural strength of about 100 kPa at maximum. The largest variation in the flexural strength within a single campaign of all the previous model-scale experiments was by Repetto et al. [18,19]. Reported results on experiments with systematic ice strength variation in a larger range do, however, not exist.

This paper provides new experimental insight on ice-structure interaction process in shallow water. The work is based on a series of model-scale experiments performed in the Aalto Ice Tank. In the experiments, an ice sheet was pushed against an inclined, 10 m wide, structure (Fig. 1a–c). The horizontal load acting on the structure was recorded and the interaction process monitored and analyzed. Three test series with different ice properties were conducted: In one of the series the compressive and flexural strength of ice was ~50 kPa; in the two other series, the ice was two and four times stronger. The ice thickness in all experiments was about 50 mm.

The novelty of the present study is the very wide structure — the ice thickness to structure width ratio was 1:200. This allows a study on a nearly two-dimensional ice accumulation process. Even if the structure is not a prototype of a real structure, its width and inclination angle are comparable to ice barriers in shallow water areas such as the Caspian Sea. As described above, previous model-scale work on shallow water ice-structure interaction have been conducted with ice having the flexural strength of about 100 kPa at maximum. We believe that such ice might lead to the ice rubble pile, forming during the interaction process, to consist of slush rather than individual ice blocks. Full-scale ice rubble piles, however, are often likely to consist of individual ice blocks, rather than slush. Thus, the ice strength in the presents study, was systematically varied in a fairly wide range, which exceeded the values in the previous laboratory-scale experiments. We also believe that, even if the effect of ice strength on the ice loads on a shallow water structure have not previously been observed, with a sufficient range of ice strengths, an effect might be found.

This paper has the following structure. Section 2 describes the experimental set-up, testing procedure, ice properties and instrumentation. Section 3 presents the results from the experiments. In Section 4, the results are analyzed, discussed, and compared with earlier studies. Section 5 ends the paper with conclusions.

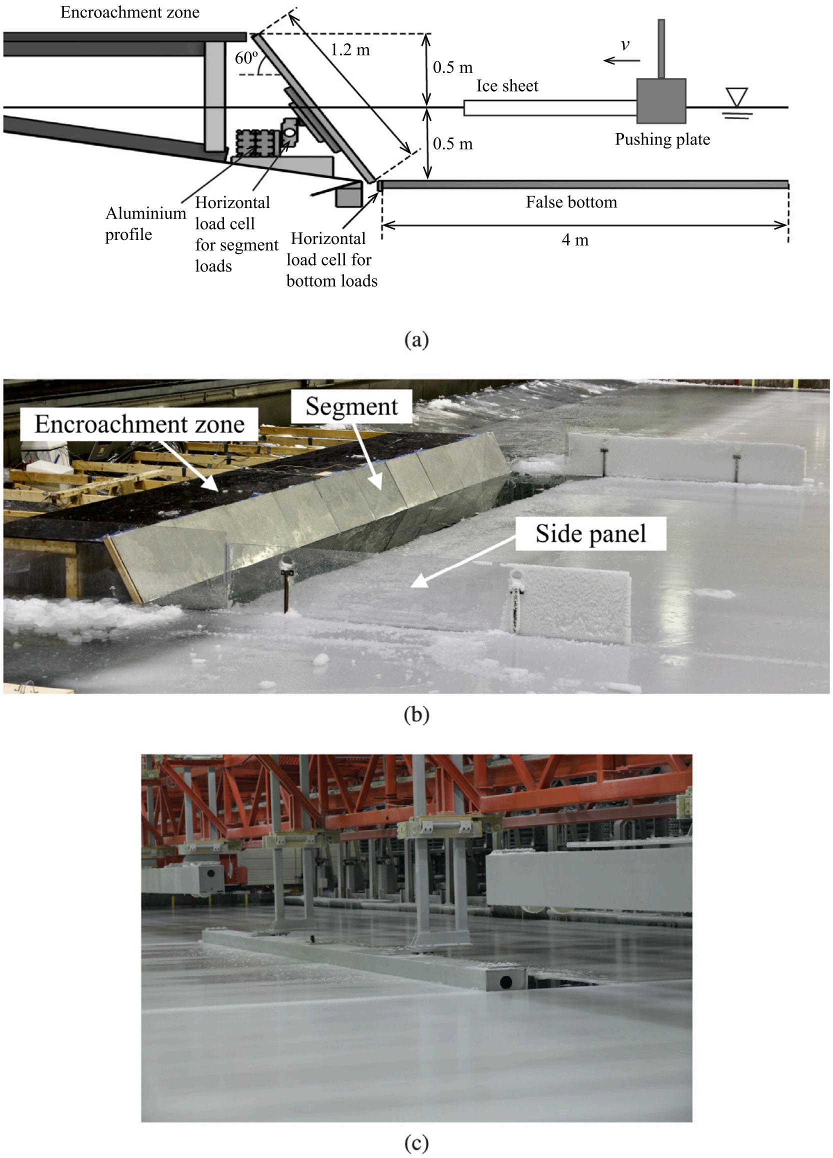

Fig. 1. Experimental set-up: (a) main dimensions and instruments, (b) general overview and (c) the pushing plate at the far end of the ice sheet strip used to move the ice.

2. Methods

2.1. Experimental set-up

The experiments were performed in the Aalto Ice Tank, equipped with a retrievable false bottom. Figs. 1a–c describe the experimental set-up and Table 1 summarizes the instruments used. The structure was 10 m wide, 1 m tall, and it had a freeboard of 0.5 m. The inclination angle of the structure was 60° and the structure width to ice thickness ratio was ~200; the structure was designed to be as wide as practically possible with a goal to mimic a two-dimensional ice accumulation scenario. The ice was moved against the structure by a pushing plate with a width equal to that of the structure (Fig. 1c). Sideways motion of the ice was constrained by vertical plexiglass panels on each side of the structure. The water depth was selected based on results from two-dimensional finite-discrete element simulations conducted by Lemström et al. [4], so that the rubble pile would have room to grow, yet also ground in all experiments.

The structure consisted of ten identical one-meter-wide segments, each mounted on an aluminum beam attached to one side of the ice basin (Fig. 1a). The segments were fabricated from 40 mm thick plywood, stiffened with extra 30 mm thick plywood

Table 1
Summary of the instrumentation used in the experiments.

Type of instrument	Model	Location	Range	Resolution [Hz]	Function
Data acquisition system	QuantumX MX410B	–	–	–	Collection of data
Horizontal load cells	HBM: PW29C3	Segments	0–1000 kg	2400	Ice loads on segments
Horizontal load cells	Tedea-Huntleigh: Model 620	False bottoms	0–500 kg	2400	Ice loads on bottoms

Table 2
Test matrix. H_i is the ice thickness, ρ_i is the ice density, σ_f is the flexural strength of the ice, σ_c is the compressive strength of the ice, E is the elastic modulus and L_{max} is the total length of ice pushed against the structure.

ID	H_i [mm]	ρ_i [kg/m^3]	σ_f [kPa]	σ_c [kPa]	E [MPa]	L_{max} [m]
W-1	50	926	44	46	107	23.2
W-2	52	928	50	51	112	19.7
W-3	52	934	42	54	103	21.6
M-1	50	916	109	121	387	25.3
M-2	51	920	108	130	328	25.9
S-1	52	915	211	214	2023	25.7
S-2	52	909	197	261	1529	24.6

and aluminum plates attached behind them. The segments were coated with 1 mm thick stainless steel sheets to provide a realistic surface for the structure. The ice-structure friction coefficient was measured to be about 0.1. The horizontal load on each segment was measured independently by a uni-axial S-shaped load cell, installed at the interface of the segment and the beam. The global load on the entire structure was taken as the sum of the ten segments. Segments and the mountings of the load cells were sufficiently stiff for the set-up to be considered rigid under the measured loads.

The false bottom reached approximately 4 m away from the structure (Fig. 1a). The bottom was made of plywood covered with a polypropylene carpet. The aim in using the carpet was to exaggerate the bottom friction in shielding the structure from ice loads. The friction coefficient between the bottom and the ice was measured to be 0.55. The horizontal load acting on the false bottom was measured by S-shaped, uni-axial load cells at its interface with the side wall of the basin. The load cells were pre-stressed to the side wall with springs. The structure was further equipped with a 1.25 m long horizontal encroachment zone (Fig. 1b).

2.2. Ice properties and test procedure

The experiments were performed with granular ice, produced following the standard techniques of the Aalto Ice Tank [8] and tempered for achieving target ice properties. The ice was grown in a continuous process, where a fine mist of 0.3% ethanol-doped water was uniformly sprayed into the $-10 \cdots -16$ °C ambient air above the basin to form ice, layer-by-layer, until the desired ice thickness was reached. The air temperature for tempering the ice was determined according to the target ice strength.

Table 2 summarizes the ice properties in the experiments which consisted of three test series: W, M, and S. In series W, ice with the flexural and compressive strength of ∼50 kPa was used, whereas in series M and S, ice with approximately two and four times higher strength, respectively, was used. The test series W, M and S are thus referred to as 'weak', 'medium' and 'strong'. Table 2 shows the ice thickness, H_i, ice density, ρ_i, flexural strength, σ_f, compressive strength, σ_c, elastic modulus, E, and the maximum length of ice pushed against the structure, L_{max}, for each experiment. The target thickness for all ice sheets was 50 mm. The ice–ice friction coefficient, measured separately in all experiments, varied between $0.1 \cdots 0.15$.

The flexural strength of the ice was measured using the in-situ cantilever beam method recommended by the International Towing Tank Conference (ITTC) [25]. Fig. 2 shows an example of the force–time curve for an experiment with ice in the W, M and S series. The dimensions of the cantilever beams follow the ITTC guidelines. The compressive strength was also measured in-situ by loading short cantilever beams axially until ice failure. The force was recorded and the compressive strength was calculated from $\sigma_c = f/bH_i$, where f is the force at failure, b the width of the ice beam, and H_i the ice thickness. The length and width of the beams in the compressive strength measurements were both equal to the ice thickness within the range of ±1 mm. The compressive strength test and measured failure load might be influenced on the beam dimensions [25] and, thus, the measured compressive strength cannot be considered as an absolute value. The elastic modulus was measured with the infinite plate test, also as recommended by ITTC and which is common practice in all model test basins. Model ice has previously been observed to exhibit non-linear behavior under flexural loading [6,9,26]. Slight non-linearity can also be observed in the graphs of Fig. 2. Furthermore, the weak ice appear to bend more before failure, than the medium and strong ice (Fig. 2). The elastic modulus could also be determined using the cantilever beam test method [25], which von Bock und Polach et al. [9] suggest that should be preferably used instead of the infinite plate method. The displacements during the flexural strength experiments were, however, not measured and the results from the cantilever beam experiments cannot be used to calculate the elastic modulus here. It should, however, be noticed that the elastic modulus determined by using cantilever beam tests might be lower than those yielded by infinite plate tests.

Before each experiment, a strip of ice of width of the structure was sawn out of the surrounding ice sheet. During an experiment, the strip was pushed against the structure with a constant velocity of 0.05 m/s. The ice sheet surrounding the strip was left in place to offer support in case the strip would have shown sideways motion. However, visual observations and the results from the experiments showed that there was virtually no contact between the pushed ice strip and the surrounding ice field. The ice edge facing the structure was cut into an irregular form (Fig. 5a and e).

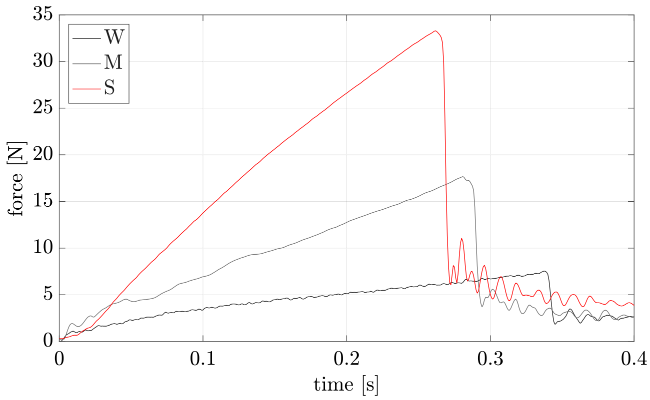

Fig. 2. Force–time plots of cantilever beam experiments with the three different ice types. The displacement was not measured in the experiments, but the velocity of the plunger was 5 mm/s.

3. Results

3.1. Load–displacement records

The horizontal ice load, F, as a function of the length of ice pushed against the structure, L, for each experiment is shown in Fig. 3. The similarity of the load records from the experiments in each series indicates good repeatability of the tests. The load records demonstrate two distinct phases: (1) At the beginning of each experiment, F increases more or less linearly. The slope of this increase was equal in all the tests. During this phase the ice sheet failed against the structure and the rubble pile in front of the structure grew. (2) The latter part of each experiment is characterized by a steady-state phase with an approximately constant ice load. Comparison of the load and video recordings of the tests showed that the steady-state phase started when the ice sheet started to fail against the edge of the rubble pile, and not against the structure anymore. The highest peak loads were measured during the second phase.

Fig. 4 shows the horizontal bottom load, F_b, for three experiments with weak, medium and strong ice. Initially, F_b is zero as the ice piling against the structure has not reached the bottom. This grounding starts at $L \approx 4$ m, and after that the loads increase monotonically until at $L \approx 8$ m they start to decrease. After $L \approx 11$ m, the load records diverge and reflect the individual failure processes. In general, the loads transmitted to the bottom are low compared with the loads on the structure. In the case of weak ice, the load on the bottom fluctuates between positive and negative values. A negative value means the load is acting away from the structure. With strong ice, at $L \approx 17$ m, an abrupt increase in F_b can be observed. This matches a sudden decrease in the load to the structure in Fig. 3(c): The ice load becomes suddenly transferred from the structure to the bottom.

3.2. Maximum and average loads

Table 3 shows the maximum loads on the structure and the bottom, F^p and ${F_b}^p$, respectively. As described in Section 3.1, the load records show two phases, an increasing load at the beginning of an experiment, followed by a steady stage. Table 3 gives also the mean load during the steady-state phase for the structure and the bottom, F^{avg} and ${F_b}^{avg}$, respectively. The beginning of the steady-state phase was estimated visually. Additionally, the table presents the ratios ${F_b}^p/F^p$ and ${F_b}^{avg}/F^{avg}$.

Table 3 shows that even if the highest loads were measured with the strongest ice, higher loads were measured with the weak ice than with the medium ice — although both the flexural and the compressive strength of the weak ice were only about half of those of the medium ice. Interestingly, the ice loads were not directly proportional to the ice strength. As will be discussed below in detail, the failure mode of the ice in this ice-structure interaction event was affected by the ice strength.

According to Table 3, the bottom loads follow the same trend as the structure loads. The peak bottom loads for test series W and S were larger than those for test series M. However, the mean bottom loads during the steady-state phase were highest for the strong ice and lowest for the weak ice. As Fig. 4 shows, with weak ice F_b fluctuated between negative and positive values, which leads to low ${F_b}^{avg}$.

If the grounded ice rubble was to protect the structure from high loads, the loads from the incoming ice sheet should be transmitted to the bottom. Table 3, however, demonstrates that both ${F_b}^p$ and ${F_b}^{avg}$ are small when compared to F^p and F^{avg}. The ratio ${F_b}^p/F^p$ varies in the range $0.16 \cdots 0.36$ and the ratio ${F_b}^{avg}/F^{avg}$ in the range $0.05 \cdots 0.36$. The bottom, thus, carried only a small portion of the horizontal load.

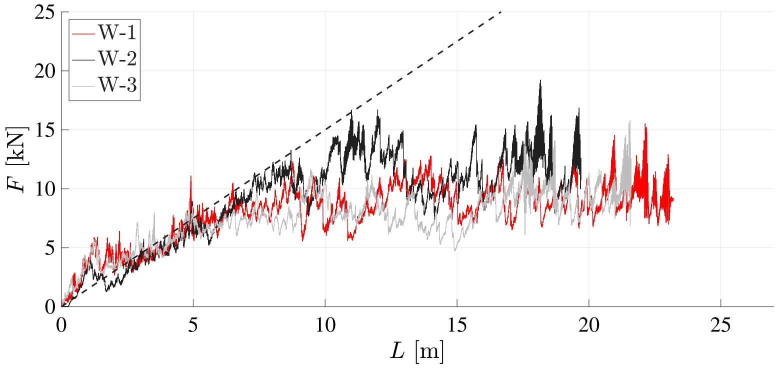

(a) Weak ice

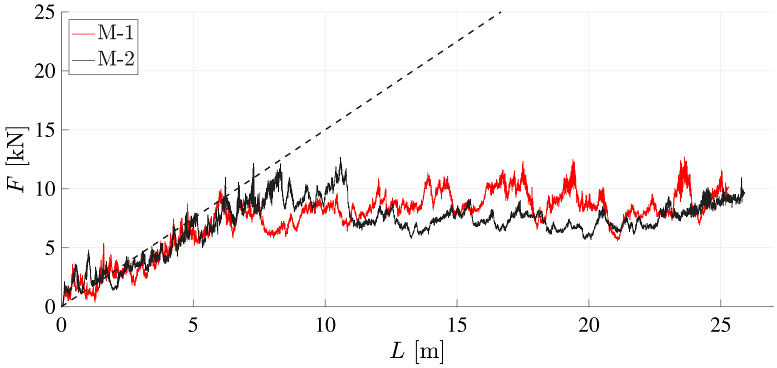

(b) Medium ice

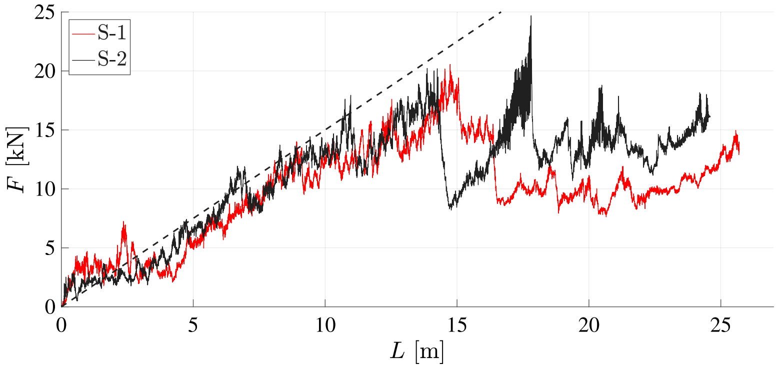

(c) Strong ice

Fig. 3. The horizontal ice load, F, plotted against the length of pushed ice, L: (a) weak, (b) medium, and (c) strong ice. The load records show two phases: First F increases linearly and then settles into a steady-state with an approximately constant value. The dashed lines in the figures will be addressed in Section 4.1.

Table 3
Measured loads. F^p and $F_b{}^p$ are the peak loads on the structure and the bottom, respectively. F^{avg} and $F_b{}^{avg}$ are the mean loads acting on the structure and the bottom during the steady-state phase of the experiment, respectively.

ID	F^p [N]	$F_b{}^p$ [N]	$F_b{}^p/F^p$	F^{avg} [N]	$F_b{}^{avg}$ [N]	$F_b{}^{avg}/F^{avg}$
W-1	15 540	4640	0.30	9190	490	0.05
W-2	19 230	3010	0.16	11 610	1830	0.16
W-3	15 790	5020	0.32	8600	390	0.05
M-1	12 700	3280	0.26	8560	1820	0.21
M-2	12 700	4600	0.36	7820	1540	0.20
S-1	20 560	5520	0.27	11 030	3920	0.36
S-2	24 690	5910	0.24	13 750	3100	0.23

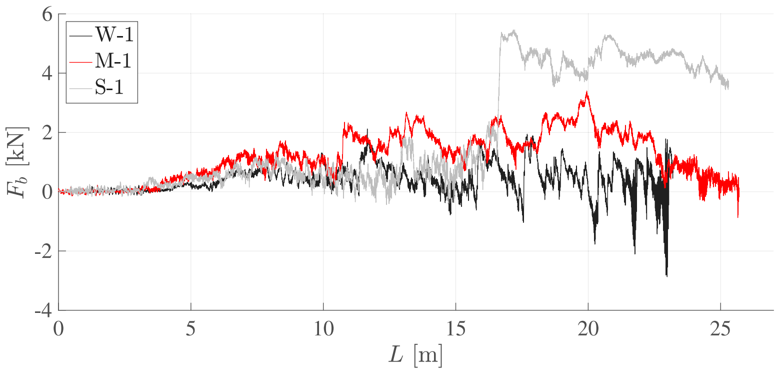

Fig. 4. The horizontal ice load on the bottom, F_b, from experiments with weak, medium and strong ice, as functions of the length of ice pushed against the structure, L.

3.3. Visual observations

Figs. 5 and 6 present snapshots from experiments W-1 (with weak ice) and S-1 (with strong ice). Additionally, examples of the morphology of the final rubble piles are presented in Fig. 7. As the figures show, the ice block size and the morphology of the rubble piles were influenced by the ice strength. Compared to test series W, the ice blocks in test series M and S were larger, and the piles were formed by distinct ice blocks and pores. The rubble piles consisted of rafted ice pieces both above and below water line (Fig. 7b). In the tests with weak ice, the top layer of the rubble consisted of small blocks but the interior of the piles consisted of a slush-like substance (Fig. 7a). The average edge-to-edge dimension of the blocks in test series W, M, and S were approximately 0.2, 0.40 and 0.5 m, respectively, while the largest measured blocks, respectively, exceeded widths of 0.6, 0.8 and 0.90 m.

Ice encroachment, the process of ice accumulating on top of the structure, occurred in all of the experiments. As Figs. 5 and 6 show, the amount of encroached ice increased with ice strength. The strong ice started to encroach soon after the start of a test due to ride-up, that is, ice fragments were pushed along the structure all the way to its top by the incoming ice, and continued until about 15 m of ice was pushed (Fig. 5). With the weak and medium ice, encroachment occurred during the intervals 4 m $< L <$ 9 m (Fig. 5) and 2 m $< L <$ 12 m, respectively. In the case of the weak ice, the encroachment occurred only through pile-up, that is, the incoming ice broke into ice blocks, which accumulated into a rubble pile that eventually reached the height of the structure. Experiments with medium and strong ice showed encroachment through both, pile-up and ride-up. As discussed in Section 3.1, the ice started to fail against the rubble pile as the steady-stage period started (Fig. 3). Logically, this also seems to be approximately the time instance, after which no more ice encroachment occurred.

3.4. Rubble pile geometries

Fig. 8 presents top and side views of the rubble piles at the end of experiments W-1, M-1 and S-1. The side profiles above water describe the average of three profiles: one from the both ends and one from the middle of the structure (points Y = 0 m, Y = 5 m and Y = 10 m of Fig. 8a). The side profiles below water illustrate the profiles at point Y = 10 m only.

As Fig. 8 shows, the rubble piles after experiments M-1 and S-1 were similar in length and height, whereas the rubble pile after experiment W-1 was shorter and slightly lower than the other two. As the amount of ice pushed into the piles is known, the rubble porosity can be estimated by using the side profiles. The rubble porosity was 0.33 for experiment W-1, whereas for M-1 and S-1, the porosity was 0.42 and 0.48 respectively. As described above, medium and strong ice led to rubble piles with distinct ice blocks, whereas the piles formed by the weak ice consisted also of very small particles, or slush (Fig. 7). Additionally, Fig. 8 shows the difference in ice encroachment between ice types. Experiment S-1 shows extensive encroachment, whereas experiment W-1 had virtually no ice on top of the structure. The geometry of the rubble piles at the end of the other experiments in the three test series were similar to the ones in Fig. 8.

Fig. 9 shows how the rubble piles grew during experiments W-1 and S-1. The side profiles illustrate the piles on the vertical plane at Y = 10 m only, that is, at the left end of the structure. There was some variation in the pile profiles throughout the structure width, but the side profiles in the figure give a fair representation of the pile geometry. For both the experiments, the volume of the rubble pile is not changing much between L = 8 m and L = 16 m. The rubble pile appears first to grow in volume, then get more compact, and then again grow in volume. This development of the rubble can also be observed in porosity, as calculated from the side profiles. At L = 8 m, the porosities are 0.46 for W-1 and 0.49 for S-1. When 16 m of ice has been pushed against the structure, the porosities are reduced into 0.21 for W-1 and 0.25 for S-1, after which the porosities increase again: into 0.33 for W-1 and into 0.50 for S-1.

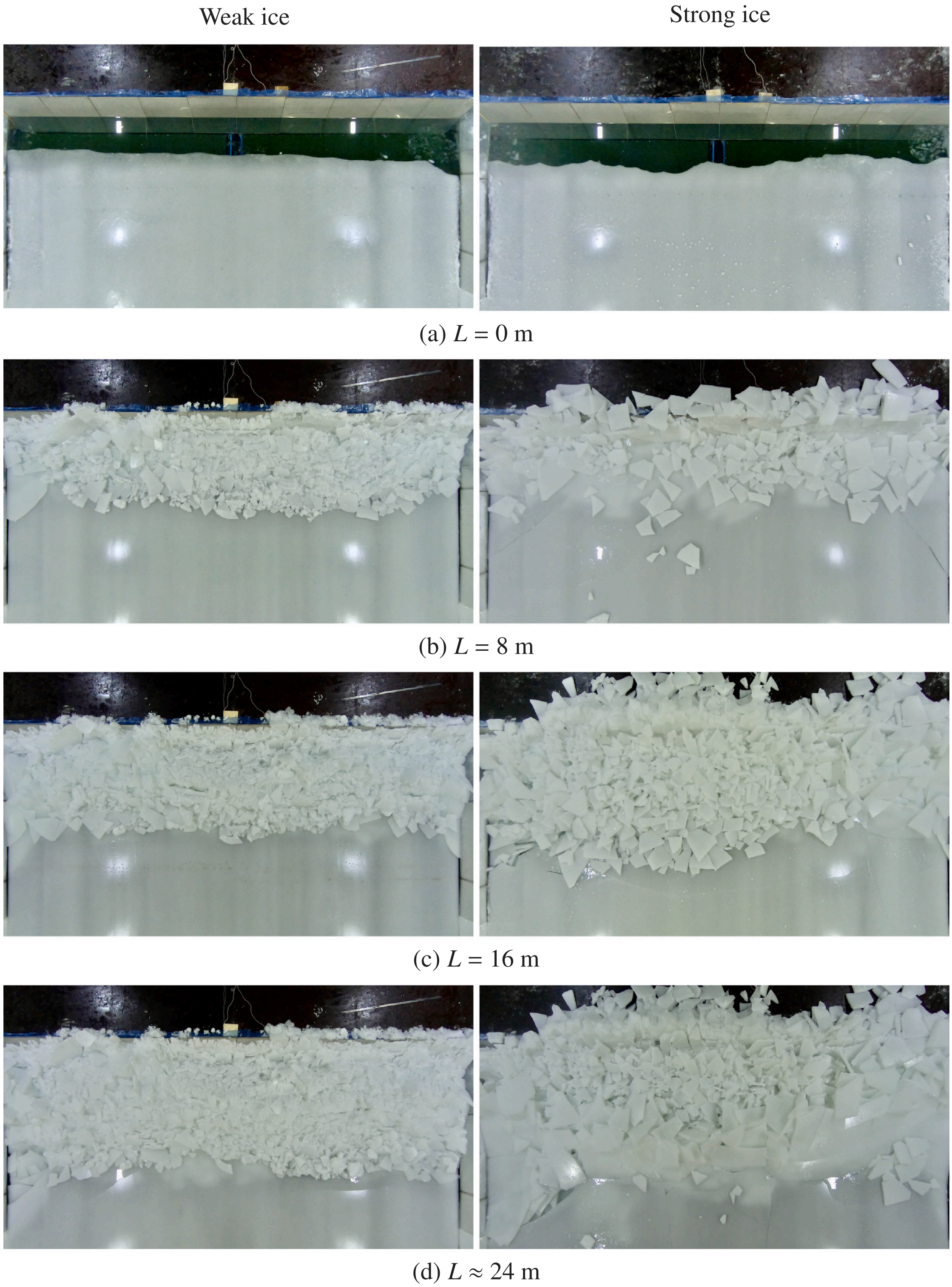

Fig. 5. Snapshots of the rubble pile-up (top view) during experiments W-1 and S-1, when 0, 8, 16 and approximately 24 m of ice has been pushed against the structure.

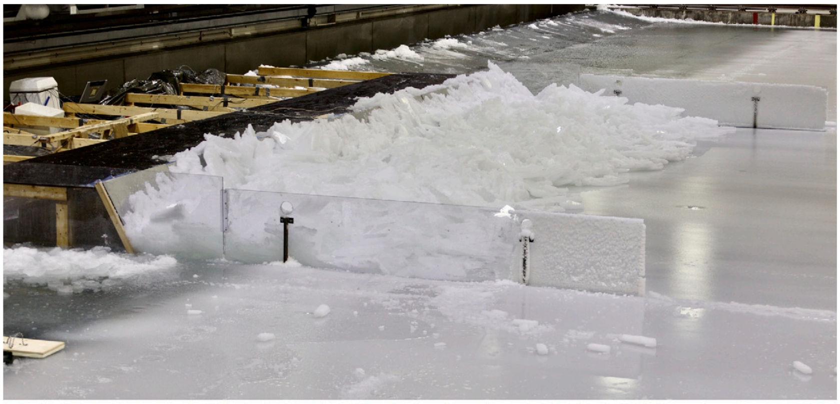

(a) Weak ice

(b) Strong ice

Fig. 6. Rubble piles at the end of experiments W-1 and S-1 performed with weak and strong ice, respectively.

(a) Weak ice

(b) Strong ice

Fig. 7. The morphology of the final rubble piles with (a) weak ice and (b) strong ice. Both figures a and b illustrate an approximately 1 m width of the rubble piles.

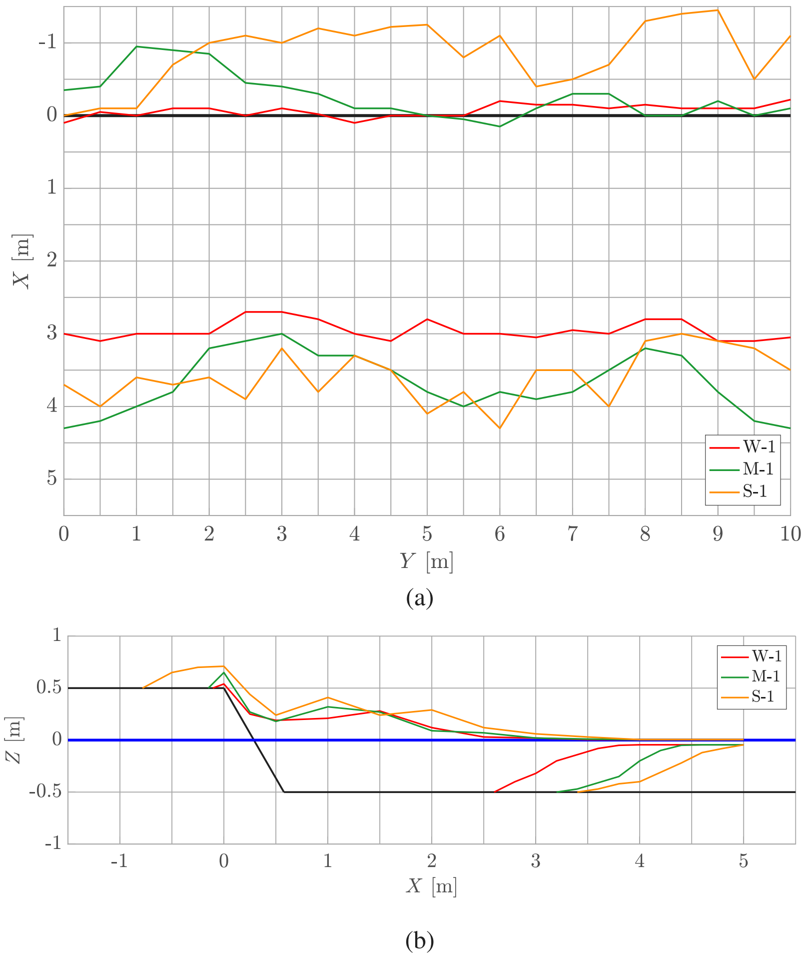

Fig. 8. Comparison of the (a) top and (b) side profiles of the rubble piles after the experiments W-1, M-1 and S-1.

4. Analysis and discussion

4.1. Load–displacement relation

All the force–displacement records in Fig. 3 show similar general features: First the force increases linearly with displacement and then stays more or less constant. For all the tests the slope of the initial linear growth stage is similar, about 1.5 kN/m, demonstrated by the dashed lines in Fig. 3. Neither the ice strength nor stiffness was affecting the slope of the initial stage. In order to elucidate this observation, Fig. 10 shows the load–displacement records in non-dimensional form. The data was made non-dimensional by following the analysis of ridging by Hopkins et al. [27]:

$$\hat{L} = L/L_c \tag{1}$$

and

$$\hat{F} = F/\rho_i g w H_i L_c, \tag{2}$$

where ρ_i is the ice density, g is the gravitational constant, w is the structure width, H_i is the ice thickness, and L_c is the characteristic length of a semi-infinite beam on an elastic foundation: $L_c = \sqrt[4]{4EH_i^3/12\rho_w g}$ [28], where ρ_w is the water density and E is elastic modulus.

As Fig. 10 demonstrates, all the tests show initially the same force–displacement relationship, $\hat{F} = C\hat{L}$, where $C \approx 0.3$. This relationship can be put into the form

$$F = C\rho_i g w H_i L, \tag{3}$$

showing that during the initial stage, the force is related to the weight of the ice mass. This result allows calculation of the $F - L$ relation during the initial stage, which a simple model illustrates in Fig. 11a. When an ice sheet has moved a distance L, a grounded

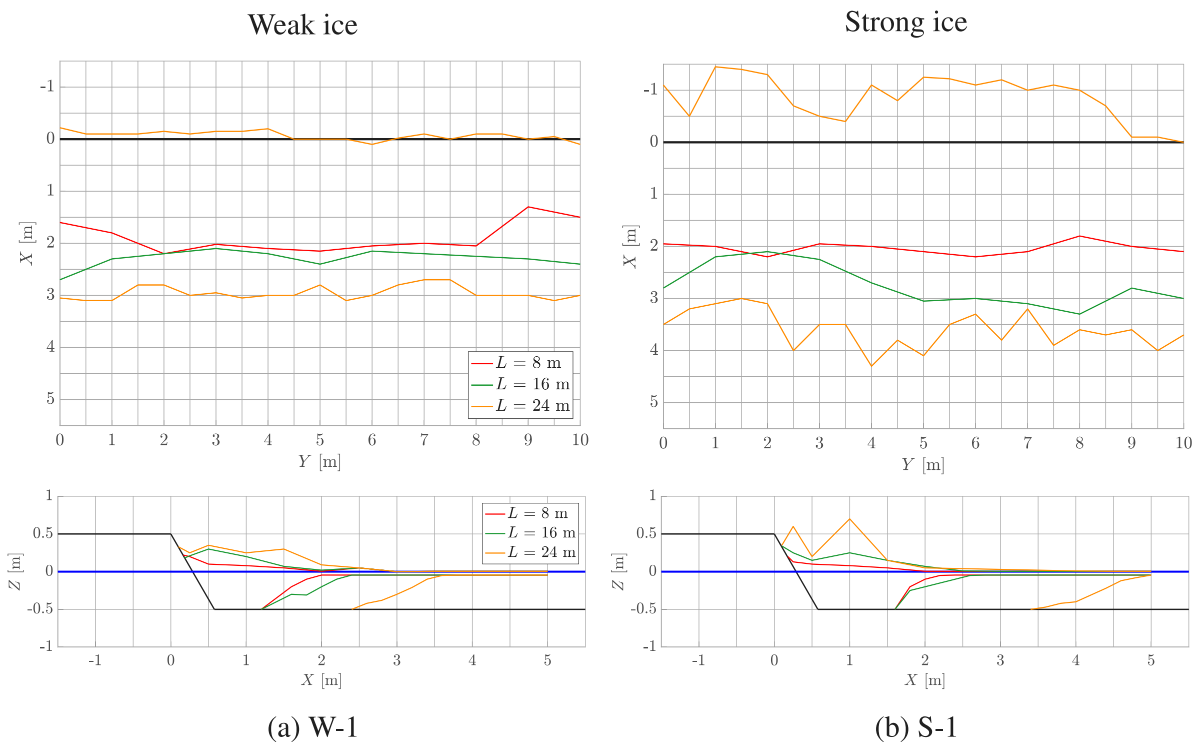

Fig. 9. The development of the rubble pile geometries. The top and side profiles of the rubble piles at three different stages of the experiments (a) W-1 and (b) S-1. The side profile is for the vertical plane at Y = 10 m (left end of the structure).

pile with the length l at the water surface has formed (see also Fig. 9). As L, ice thickness, H_i, and water depth, d, are known, l can be estimated. First, $LH_i \sim dl'$ leading to $l' \sim 0.1L$ (here $d/H_i = 0.1$), where l' is as shown in Fig. 11a. Then, by taking the shape of the ice pile, the porosity, and the volume of ice above the water into account, we can make an engineering assumption that $l = 0.2L$.

When an ice sheet is breaking against the structure in shallow water, the grounded rubble pile inhibits the downwards motion of the sheet and may force it to move upwards together with the ice blocks that are laying on it. Based on visual observations, Figs. 5b and 9, it can be estimated that the volume of ice on top of the sheet is wH_il and that the volume has a triangular shape, leading to the model shown in Fig. 11b: a vertical force, F_v, is needed to lift up the floating ice sheet and the ice blocks resting on top of it. Using the equations shown in Fig. 11b, it can be calculated that $F_v = 3400l$ [N/m] and that lifting the ice blocks on the ice sheet takes about 90% of the force. The horizontal force on the structure due to F_v can be calculated as the slope of the structure, α, and the friction between the ice and the structure, μ_s, are known:

$$F_g = \frac{\sin\alpha + \mu\cos\alpha}{\cos\alpha - \mu\sin\alpha} F_v \quad \Rightarrow \quad F_g = 2.2F_v \quad \Rightarrow \quad F_g = 7557l \quad \Rightarrow \quad F_g \approx 1500L \text{ [N/m]}, \tag{4}$$

where α = 60°, μ_s = 0.1, and l = 0.2L have been used. In addition to this gravitational force, there are frictional forces acting horizontally; $F_{\mu 1}$ between the moving ice sheet and the grounded pile and $F_{\mu 2}$ between the moving ice sheet and the ice blocks on top of the ice sheet. Both the frictional forces are shown in Fig. 11b and by taking $\mu_i = 0.1$,

$$F_\mu = F_{\mu 1} + F_{\mu 2} \quad \Rightarrow \quad F_\mu = 530l + 451l = 981l \quad \Rightarrow \quad F_\mu \approx 200L \text{ [N/m]}, \tag{5}$$

where again $l = 0.2L$. Finally

$$F = F_g + F_\mu \approx 1700L \text{ [N/m]}, \tag{6}$$

which is close to the relation $F \approx 1500L$ [N/m] measured during the experiments and shown in Fig. 3. The model outlined above and illustrated in Fig. 11 included a number of simplifications, but it is important to note that about 90% of the force is due to weight of the ice lifted upwards. The initial slopes of all the tests are similar because the dimensions and density were the same in all the tests, and thus the weights were the same.

In addition to the equal initial slopes, Fig. 10 shows that the non-dimensional forces cease to increase and settle to an approximately constant value at $\hat{F} = 1.8 \cdot 10^{-3}$ for the S and M series, but at $\hat{F} = 3 \cdot 10^{-3}$ for the W series. Why does the load stop following the initial linearly increasing trend and settle into a more or less constant value? Why is this value similar for the S and M series, but higher for the W series, the weakest ice?

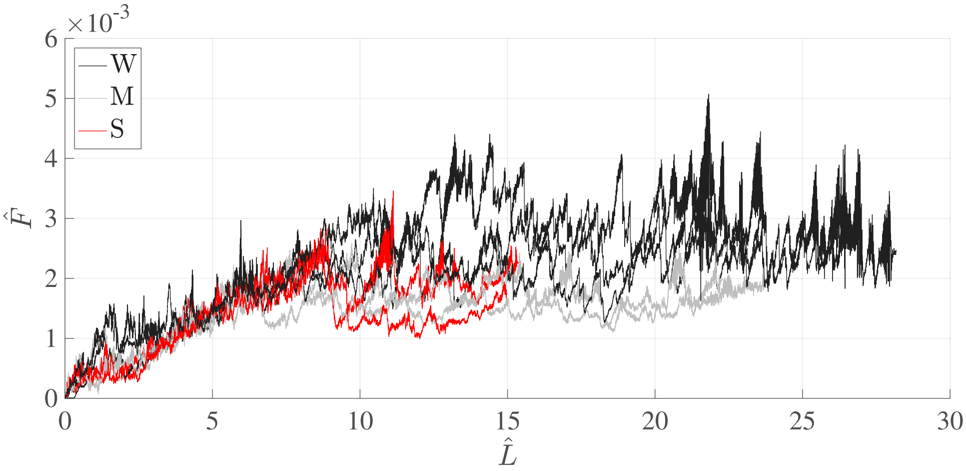

Fig. 10. Normalized force, $\hat{F}$, as a function of normalized length of ice pushed against the structure $\hat{L}$.

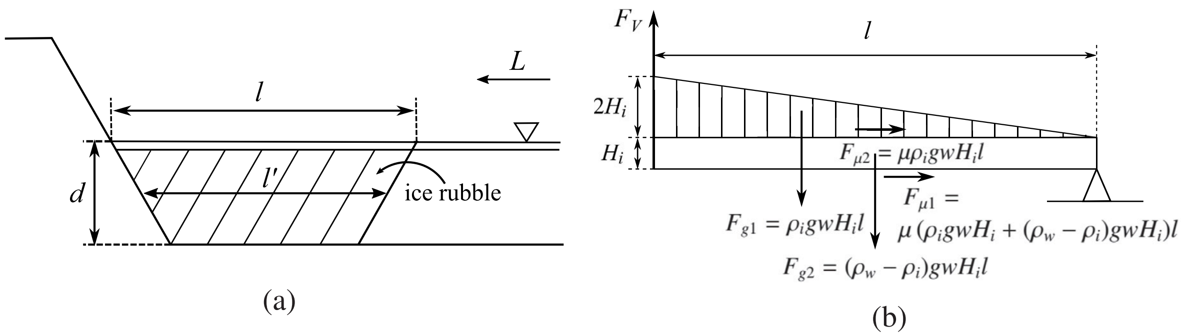

Fig. 11. The model. When an ice sheet has moved a distance L, a grounded pile with length l at the water surface has formed, and since L, H_i and d are known, l can be estimated according to Figure (a). Figure (b) illustrates the components of the vertical force, F_v, and their equations, needed to lift the floating ice sheet and the ice blocks resting on top of it.

The ratio of the dimensional loads during the steady-state phase, F_{avg} (Table 3), of test series S and M is equal to the ratio of the average characteristic lengths of the ice used in the S and M series: $F_{avgS}/F_{avgM} = L_{cS}/L_{cM} = 1.5$. The ratio of both the bending and compressive strengths in the S and M series is higher: $\sigma_S/\sigma_M = 1.9$. The result that the constant part of the load during the steady-state phase can be made non-dimensional by using the characteristic length, but not by using strength, suggests that the ice failure process at this stage is dominated by buckling. For test series S and M, Fig. 10 thus indicates an interesting conclusion. When these ice sheets were breaking against an inclined structure, the load was initially dominated by the weight of broken ice pieces and later by buckling; the strength of the ice sheet appears not to have affected the ice load. Fig. 3 and Table 3 show higher loads for the stronger ice, but for the stronger ice also the elastic modulus and thus the buckling load were higher. It should be noted that the value for the elastic modulus used in this investigation was determined based on the infinite plate test.

Does all this then suggest that the strength of ice does not affect the ice load? No it does not. It suggest that the strength of ice is one of the parameters – together with ice thickness, elasticity, friction, etc. – that define what the dominant ice failure mode is. In test series W, the ice failed in a different manner than in series M and S and the non-dimensional load for the W series was higher than for the M and S series (Fig. 10); even the dimensional load for the W series was higher than the load for the M series, although both the strength and modulus in the M series were higher. According to the force records from the cantilever beam tests (Fig. 2), the weak ice was deforming more before the failure than the two other ice types, which could affect its failure process.

4.2. Scaling of model-scale results

The purpose of these experiments was not to scale the ice properties in any particular way to study full-scale ice loads, but rather to observe changes in the ice loading process as the ice properties vary. It is, anyhow, worth discussing what kind of full-scale values the experiments would scale to by using the traditional scaling approach, which is frequently used in model test basins [29]. This scaling apply geometric scaling, while fulfilling Froude and Cauchy scaling laws [26]. Froude scaling considers inertia and gravity, which Palmer and Dempsey [30] claim are of very little significance, when ice is moving slowly against a stationary structure. While

Table 4
Values of the measured ice properties and horizontal structure loads in model- and full-scale. The full-scale values are scaled using geometric scaling and the scaling factor, λ, was selected so that σ_f for all experiments in full-scale was 600 kPa.

ID	λ	Model-scale: $v = 0.05$ m/s					Full-scale: $\sigma_f = 600$ kPa				
		σ_f [kPa]	σ_c [kPa]	H_i [m]	E [MPa]	Line load [kN/m]	σ_c [kPa]	H_i [m]	E [MPa]	Line load [kN/m]	v [m/s]
W-1	13.6	44	46	0.050	107	1.6	626	0.68	1455	287	0.18
W-2	12.0	50	51	0.052	112	1.9	612	0.62	1344	277	0.17
W-3	14.3	42	54	0.052	103	1.6	772	0.77	1473	323	0.19
M-1	5.5	109	121	0.050	387	1.3	666	0.28	2129	38	0.12
M-2	5.6	108	130	0.051	328	1.3	728	0.28	1837	40	0.12
S-1	2.8	211	214	0.052	2023	2.1	599	0.15	5664	16	0.08
S-2	3.0	197	261	0.052	1529	2.5	783	0.16	4587	22	0.09

this is a valid argument and demonstrates challenges related to scaling, it is not the intention of this paper to address the validity of the method, but merely utilize this frequently used scaling technique to discuss the results further.

Table 4 presents the model-scale values of σ_f, σ_c, E and of the line load. The line load is defined as the maximum load on the structure, divided by the width of the structure. Since the model-scale structure did not have any full-scale equivalence, no actual scale exist, but for the purpose of this investigation, the scaling factor, λ, for each experiment was selected so that the flexural strength for all the experiments in full-scale was 600 kPa. The full-scale ice properties, line load and ice drift velocities, v, obtained with these assumptions are given in Table 4.

It is ambiguous whether the above-described scaling leads to accurate estimates of full-scale ice load magnitudes, but assumed that it does, the experiments conducted can be interpreted as model-scale experiments at different scales. Test series S can be interpreted as studying 0.15 m thick ice, while test series M was studying 0.3 m thick ice with similar strength but lower stiffness. In full-scale, both are rather thin ice and could well be failing through buckling. Test series W can be interpreted as studying 0.7 m thick ice with low stiffness; soft ice that can be easily compressed. All these combinations of full-scale ice properties are different, but they all are realistic. When planning model-scale experiments, it is important to consider that the model ice properties affect the failure process of the ice and care must be used when interpreting the results.

4.3. Grounding and bottom loads

A grounded pile is often assumed to protect a shallow water structure by transmitting portion of the loads to the bottom. Here this type of protective effect, however, appeared to be weak: Both the mean and the peak horizontal loads applied on the bottom were 5 ⋯ 36% of those induced on the structure (Table 3). This result agrees well with the results from two-dimensional finite-discrete element simulations conducted by Lemström et al. [4], who observed a ratio $F_b{}^p/F^p$ of approximately 14% with a similar water depth to ice thickness ratio. Earlier work [1–3] suggests that a grounded rubble pile protects the structure from high ice loads. These studies suggested an up to 85% reduction in the peak ice loads, when a grounded rubble pile was present.

As Lemström et al. [4] discussed, the maximum ice loads are likely to occur in a pristine, continuous, ice loading process. The experiments here mimic this type of process. In the full-scale measurements reported by Marshall et al. [1], Timco and Wright [2] and Sudom and Timco [3], the rubble piles had already become stable and consolidation had occurred. Thus, it is important to consider it as a different case than the scenario of the experiments considered in this paper. In model-scale experiments on a Caisson-type platform by Karulin et al. [16], it was observed that during the initial part of the interaction process, the loads in shallow water were higher than in deep water. The experiments were, however, conducted in much smaller scale than the experiments here, as the structure had the width of 1.2 m while the water depth varied between 0.13 and 0.25 m. Further, the ice thickness in their experiments was only 1–2 mm and the flexural strength of the ice 10 kPa. Saarinen [31] conducted ice-inclined structure tests on a 5 m wide structure in deep water and found that the ice rubble pile, formed by a breaking ice sheet, sequentially formed an above-water part growing in size until it slid down along the structure and failed the ice sheet in bending downwards. In his experiments, he used the same structure inclination angle and similar ice thicknesses to the experiments here, while the ice strength was similar to the weak ice of this paper. Similar observations of ice rubble sliding downwards and breaking the incoming ice sheet was also made in two-dimensional finite-discrete element simulations by Paavilainen et al. [32]. In our experiments such downward motion and subsequent failure of the incoming ice sheet did not occur, which is likely due to the grounded rubble inhibiting the downward motion. It is suggested that this reason led to the load increase in shallow water compared to deep water observed by Karulin et al. [16]. Further, the experiments by Karulin et al. [16] showed a load reduction once a stationary grounded rubble pile had formed. Here no load reduction was observed, yet it was evident that the loading process changed during the experiment, as the incoming ice sheet started to fail against the ice rubble pile instead of breaking against the structure.

Timco et al. [15] studied the load distribution through a newly-formed grounded rubble pile by performing model tests on a vertical-sided structure built above a submerged, horizontal berm, determining the apportioning through the rubble pile on the structure and the berm. The study focused on short ice loading events only and the results showed that small horizontal forces were transmitted to the berm, but as the applied force increased, the load became mainly transmitted to the structure. The ratio between the loads acting on the berm and the total applied horizontal load for an individual loading event ranged almost all the way from 0 to 1, but in general, were higher than for the experiments here. Since Timco et al. [15] considered short loading events only, had a vertical-side structure and the water depth to ice thickness ratios significantly lower than in the experiments, direct comparison of the results is challenging.

4.4. Encroachment

In the experiments, the encroachment was influenced by the ice properties (Fig. 8a). This finding is in line with the model-scale tests on ice loading process on shallow water structures by Bridges et al. [24], who observed similar increase in the maximum encroachment height and length with increasing ice strength. They suggested that low ice compressive strength may prohibit force chains from forming and, thus, ice encroachment from occurring. In agreement with the results of this paper, their experiments showed that ice block sizes increased with ice strength. As in the experiments here, the flexural strength, the compressive strength and the elastic modulus were varied simultaneously and, thus, the effect of each individual material parameter could not be determined. On the contrary to here, Repetto et al. [19] did not observe a clear effect of the flexural strength on the ice block size and breaking length. However, the ice thickness and the flexural strength were varied simultaneously and a direct relationship between the flexural strength and the block size was not easy to observe. In addition to this, discrete element simulations by Bridges et al. [33] suggested that ice encroachment increased with flexural strength of ice.

5. Conclusions

Laboratory-scale experiments on shallow water ice-inclined structure interaction process, in the case of grounded rubble piles, were performed. In the experiments, a ten-meter-wide ice sheet was pushed against an inclined structure of the same width. In total, seven experiments were performed. The ice thickness was about 50 mm in all experiments. The experiments showed good repeatability between the tests within each test series. The main findings of the paper are:

- The ice loading process on inclined structures in shallow water consists of two distinct phases (Section 3.1): (1) an initial phase with a linearly increasing ice load due to increase in ice mass above water line and (2) a steady-state phase with an approximately constant load.
- The magnitude of the ice loads induced in shallow water ice-structure interaction was not directly proportional to ice strength: The weakest model-scale ice yielded higher loads than the ice having twice its strength (Section 3.2).
- Main features of the loading process could be captured by a model developed based on normalized load data (Section 4.1). The model highlights how the weight of the ice rubble forming in the process dominates the ice load during phase (1), while buckling explains the load levels of phase (2) if the ice is strong enough. The failure process for the weakest ice was different than that the other ice types.
- The rubble pile grounded in all the experiments (Figs. 8 and 9), but only a small portion of the loads was carried by the bottom. However, the bottom may have changed the ice failure process compared to deep water by inhibiting the ice from failing downwards, thus potentially increasing the load on the structure.

The simple model developed in this paper describes the loading process with a fair accuracy. More detailed studies are, however, still needed to establish thorough understanding of the whole ice-inclined structure interaction process. Further, the ice load distribution of the experiments is of interest and will be addressed in our future study.

Declaration of competing interest

The authors declare that they have no known competing financial interests or personal relationships that could have appeared to influence the work reported in this paper.

Acknowledgments

IL wishes to acknowledge the financial support from Alfred Kordelin Foundation, Finland, and from Aker Arctic Technology Inc., Finland and Finnish Maritime Foundation through the Industry-Academia Graduate School in Aalto University Department of Mechanical Engineering, Finland. The authors are also grateful for the financial support from Business Finland, Aker Arctic Technology Inc., Finland, ABB Marine, Arctia Shipping, Finland, Technip Offshore Finland Oy, Suomen Hyötytuuli Oy, Finland, Finnish Transport Agency and Ponvia Oy through the ARAJÄÄ research-project. The authors express their appreciation to Aalto Ice Tank staff Otto Puolakka, Teemu Päivärinta and Lasse Turja for their work on the experiments.

References

[1] Marshall A, Croasdale K, Frederking R, Jordaan I, Nadreau J. Measurements of load transmission through grounded ice rubble. In *Proceedings of the 11th international conference on port and ocean engineering under arctic conditions*, St. John's, Canada, 1989.
[2] Timco G, Wright B. Load attenuation through grounded ice rubble at Tarsuit Island. In *Proceedings of the 15th international conference on port and ocean engineering under arctic conditions*, Helsinki, Finland, 1999.
[3] Sudom D, Timco G. Load reduction due to grounded ice rubble on the Molikpaq. In *Proceedings of the 20th international conference on port and ocean engineering under arctic conditions*, Espoo, Finland, 2009.
[4] Lemström I, Polojärvi A, Tuhkuri J. Numerical experiments on ice-structure interaction in shallow water. Cold Reg Sci Technol 2020;176:103088.
[5] Riska K, et al. Assessment of ice model testing techniques. In *Sname international conference and exhibition on performance of ships and structures in ice (icetech)*, Calgary, Canada, 1994.
[6] von Bock und Polach RUF. Numerical analysis of the bending strength of model-scale ice. Cold Reg Sci Technol 2015;118:91–104.
[7] Zufelt JE, Ettema R. Model ice properties. Tech. rep. 96–1, Crrel report, 1996.

[8] Li Z, Riska K. Preliminary study of physical and mechanical properties of model ice. Tech. rep. Technical report M-212, Helsinki University of Technology; 1996.

[9] von Bock und Polach RUF, Ettema R, Gralher S, Kellner L, Stender M. The non-linear behavior of aqueous model ice in downward flexure. Cold Reg Sci Technol 2019;165:102775.

[10] von Bock und Polach RUF, Ehlers S, Kujala P. Model-scale ice – part a experiments. Cold Reg Sci Technol 2013;94:53–60.

[11] Barker A, Timco GW. Maximum pile-up hights for grounded ice rubble. Cold Reg Sci Technol 2017;135:62–75.

[12] Neth V. Ice rubble formation along the Molikpaq. In *Proceedings of the 11th international conference on port and ocean engineering under arctic conditions*, St. John's, Canada, 1991.

[13] McKenna R, Stuckey P, Fuglem M, Crocker G, McGongial D, Croasdale K, Verlaan P, Abuova A. Ice encroachment in the North Caspian Sea. In *Proceedings of the 21st international conference on port and ocean engineering under arctic conditions*, Montreal, Canada, 2011.

[14] Yoshimura N, Inoue M. Model tests of ice rubble field around a gravel island. In *Proceedings of the 8th international conference on port and ocean engineering under arctic conditions*, Narssarssuaq, Greenland, 1985, p. 716–26.

[15] Timco GW, Sayed M, Frederking R. Model tests of load transmission through grounded ice rubble. In *8th international conference on offshore mechanics and arctic engineering, Vol. 1*, The Hague, Netherlands, 1989, p. 269–74.

[16] Karulin E, Karulina M, Blagovidov L. Ice model tests of caisson platform in shallow water. Int J Offshore Polar Eng 2007;17(4):270–5.

[17] Evers K, Weihrauch A. Design and model testing of ice barriers for protection of offshore structures in shallow water during winter. In *Proceedings of the 17th iahr international symposium on ice*, Saint Petersburg, Russia, 2004.

[18] Repetto-Llamarez A, Gürtner A, Gumestad O, Høyland K. Qualitative description of a should ice barrier-ice interaction during model tests. In *Proceedings of the asme 28th international conference on ocean, offshore and arctic engineering*, Honolulu, Hawaii, 2009.

[19] Repetto-Llamarezrepe A, Gudmestad O, Gürtner A, Gumestad O, Høyland K. Shoulder ice barrier ice tank testing part II: Estimation of breaking length and block size using image analysis. In *Proceedings of the asme 28th international conference on ocean, offshore and arctic engineering*, Honolulu, Hawaii, 2009.

[20] Serré N, Høyland K, Lundamo T, Bonnemaire B, Evers K, Gürtner AA. Rubble ice transport on Arctic offshore structures (RITAS), part I: Scale-model investigations of level ice action mechanisms. In *Proceedings of the 22nd International Conference on Port and Ocean Engineering under Arctic Conditions*, Espoo, Finland, 2013.

[21] Serré N, Lu W, Høyland K, Bonnemaire B, Borge J, Evers K. Rubble ice transport on Arctic offshore structures (RITAS), part II: 2DScale-model study of the level ice action. In *Proceedings of the 22nd international conference on port and ocean engineering under arctic conditions*, Espoo, Finland, 2013.

[22] Lu W, Serré N, Høyland K, Evers K. Rubble ice transport on Arctic offshore structures (RITAS), part IV: Tactile sensor measurement of the level ice load on inclined plate. In *Proceedings of the 22nd international conference on port and ocean engineering under arctic conditions*, Espoo, Finland, 2013.

[23] Timco GW. Model tests of ice forces on a wide inclined structure. In *Iahr ice symposium*, Hamburg, Germany, 1984, p. 87–95.

[24] Bridges R, Riska K, Schroeder C. Model tests for ice encroachment and formation of rubble ice. In *Proceedings of the 23rd IAHR International Symposium on Ice*, Ann Arbor, Michigan, USA, 2016.

[25] ITTC. Recommended procedures and guidelines: Testing and extrapolation methods - test methods for model ice properties. 2002, p. No. 7.5–02–04–02.

[26] Schwartz J. New developments in modelling ice problems. In *Proceedings of the 4th international conference on port and ocean engineering under arctic conditions*, St. John's, Canada, 1977, p. 45–61.

[27] Hopkins MA, Tuhkuri J, Lensu M. Rafting and ridging of thin ice sheets. J Geophys Res 1999;104(C6):13605–13.

[28] Hetényi M. Beams on elastic foundation: theory with applications in the fields of civil and mechanical engineering. Ann Arbor: The University of Michigan Press; 1979.

[29] ITTC. General guidence and introduction to ice model testing. 2017, p. No. 7.5–02–04–01.

[30] Palmer A, Dempsey J. Model tests in ice. In *Proceedings of the 9th international conference on port and ocean engineering under arctic conditions*, Luleå, Sweden, 2009, p. 1–10.

[31] Saarinen S. Description of the pile-up process of an ice sheet against an inclined plate (MA thesis), Espoo, Finland: Helsinki University of Technology; 2000.

[32] Paavilainen J, Tuhkuri J, Polojärvi A. 2D numerical simulations of ice rubble formation process against an inclined structure. Cold Reg Sci Technol 2011;68(1–2):20–34.

[33] Bridges R, Riska K, Hopkins M, Wei Y. Ice interaction processes during ice encroachment. Mar Struct 2019;67:102629.